V[subscript OC] enhancement in polymer solar cells with isobenzofulvene–C[subscript 60] adducts

V_{OC} Enhancement in Polymer Solar Cells with Isobenzofulvene–C_{60} Adducts.

Ggoch Ddeul Han[a,1], Andrea Maurano[b,1], Jonathan G. Weis[a], Vladimir Bulović[b,*], Timothy M. Swager[a,*]

[a]Department of Chemistry, Massachusetts Institute of Technology, Cambridge, MA 02139, United States,

[b]Research Laboratory of Electronics, Massachusetts Institute of Technology, Cambridge, MA 02139, United States

*Corresponding Authors:

tswager@mit.edu (T.M. Swager), bulovic@mit.edu (V. Bulovic).
[1]These authors contributed equally.

KEYWORDS Organic Photovoltaics, Bulk Heterojunction Active Layer, Isobenzofulvene, Functionalized Fullerenes, High Voc

Abstract

We report the use of isobenzofulvene–C_{60} adducts in bulk heterojunction organic solar cells, synthesized via the [4+2] cycloaddition of C_{60} with an in situ generated isobenzofulvene intermediate. The LUMO energy levels of these adducts are 20–180 meV higher than that of PCBM ([6,6]-phenyl-C61-butyric acid methyl ester). This large increase of the LUMO level is attributed to cofacial π-orbital interactions between the fullerene surface and the isobenzofulvene π–system (aromatic ring and double bond). Raised LUMO levels of fullerenes, together with their desirably slow recombination dynamics, led to higher open-circuit voltages (V_{OC}) in bulk heterojunction polymer solar cells (up to 0.75 V for bisadducts) relative to cells tested in parallel using the well-known PCBM as the fullerene acceptor. In addition to enhanced V_{OC}, the short-circuit current densities (JSC) were improved in the devices containing the epoxide analogs of the isobenzofulvene–C_{60}. Notably the epoxide derivative of the monoadduct (IBF–Ep) exhibited ~20% enhancement of power conversion efficiency (PCE) compared to reference P3HT:PCBM solar cells. A combination of optical and electronic methods was used to investigate the origin of the PCE enhancement observed with these new fullerene acceptors with particular attention to the increased V_{OC}s.

1. Introduction

Polymer solar cells with bulk heterojunction (BHJ) active layers continue to be a focus in organic photovoltaic research as a result of their large interfacial area to volume ratio, modularity, and ease of fabrication.[1–4] These solar cells however exhibit power conversion efficiencies (PCE) well below their theoretical limit. A promising approach to increase the PCE lies in the open-circuit voltage (V_{OC}), which is roughly proportional to the effective band gap between the p- and n-type materials ($HOMO_p$–$LUMO_n$).[5,6] Research on new p-type conjugated polymers has progressed considerably in recent years. The optimization of transport and tailoring of optical band gaps to capture the majority of the solar spectrum has resulted in remarkable increases of both V_{OC} and short-circuit current density (J_{SC}).[5,7,8] However, there have not been parallel improvements with the synthesis of new n-type acceptors. These efforts have mainly focused on small molecules and fullerenes designed to electronically complement their p-type counterparts.[9] Among n-type molecules, covalently functionalized fullerenes such as [6,6]-phenyl-C_{61}-butyric acid methyl ester (PCBM) and indene–C_{60} bisadducts (ICBA) are currently the most widely used. In particular, notably high V_{OC} of poly(3-hexylthiophene) (P3HT):ICBA BHJ solar cells have been attributed to the high-lying LUMO level of ICBA.[10] As a result, designing prospective n-type materials with LUMO levels that produce high V_{OC} when matched with appropriate

p-type polymers is currently one of the most promising approaches to increasing PCEs of polymer solar cells.

Most covalently functionalized fullerenes have decreased electron affinities (raised LUMOs) as a result of the reduced π-delocalization by the removal of double bonds.[11] In addition, the extent of this change can be influenced by both the structural properties of the functionalized fullerenes and the specific electronic properties of the attached functional groups. For example, we previously demonstrated with tetraalkylcyclobutadiene–C_{60} adducts[12] that cofacial interactions between C_{60} and π–orbital of the pendant group induce a significant upshift of the fullerene's LUMO energy level. Another class of materials, indene–C_{60} adducts, also displays π-orbital interactions between the aromatic ring and the C_{60} π-surface, which results in an improved V_{OC} and PCE when blended with P3HT in solar cell devices.[10] As a consequence, a new class of materials (isobenzofulvene–C_{60} or IBF–C_{60}), which contains both a strong alkene–fullerene interaction similar to the tetraalkylcyclobutadiene–C_{60} adducts as well as an aromatic–fullerene interaction similar to the indene–C_{60}s, is expected to result in even more raised LUMO levels and consequently higher V_{OC}s. Along these lines, Tseng et al. recently reported the syntheses of isobenzofulvene–fullerene monoadducts decorated with solubilizing alkyl ester groups with LUMO levels raised about 20 meV higher than PCBM. Although the raised LUMO levels resulted in improved V_{OC} by 10–30 mV compared to PCBM, their overall photovoltaic performances were lower than the standard PCBM cells.[13] In a recent study,[14] we used an epoxidized isobenzofulvene–C_{60} derivative (IBF–Ep) as an electron transport material in $CH_3NH_3PbI_{3-x}Cl_x$ perovskite planar heterojunction (PHJ) solar cells, which demonstrated the versatility of the fullerene derivative. IBF–Ep, which possesses an epoxidized alkene group that increases the solubility, and can also potentially result in larger V_{OC} and J_{SC} when used as an electron acceptor for BHJ solar cells.

In the present study, we designed and systematically investigated mono- and bisadducts of isobenzofulvene–C_{60} derivatives that have raised LUMO levels and slow recombination dynamics in the blends, which synergistically improved V_{OC} significantly. We report the syntheses and characterization of monoadducts (IBF–Mono and its epoxide derivative IBF–Ep) elsewhere and their utility in perovskite solar cells. Herein, we expand our investigations to bisadducts (IBF–Bis and its epoxide derivatives IBF–Bis–Ep1 and IBF–Bis–Ep2). We explored both the mono- and bisadducts in BHJ solar cells with P3HT as an electron donor in an effort to produce enhanced $V_{OC.}$ Furthermore, we investigate the effect of epoxide derivatives (IBF–Ep, IBF–Bis–Ep1 and IBF–Bis–Ep2) on BHJ solar cell performance through enhancements in J_{SC}.

2. Results and Discussion

2.1. Syntheses and Characterization of Isobenzofulvene–C_{60} Bisadducts

IBF–Bis was synthesized by [4+2] cycloaddition reactions of an intermediate 8,8-dimethylisobenzofulvene[15] with the IBF-mono adduct (Scheme 1 (a)). IBF–Bis is a mixture of regioisomers as revealed by ^{1}H and ^{13}C nuclear magnetic resonance (NMR) spectra (Figure S1). These bisadducts exhibit enhanced solubility relative to IBF–Mono in dichloromethane, chloroform, toluene, chlorobenzene, and *o*-dichlorobenzene, and are easily purified by HPLC using a 5PBB Cosmosil column with toluene elution. The disruption in the π-system by two successive cycloaddition reactions produces raised LUMO energy levels,[16,17] which in turn translates to higher V_{OC} compared to those of the monoadducts. Epoxide derivatives of IBF–Bis were synthesized and expected to retain part of the LUMO offset energy of IBF–Bis and to have improved solubility as a result of the polar nature of the epoxide (Scheme 1 (b), (c)). For optimal yields and ease of purification, IBF–Bis–Ep1 was synthesized by appending an isobenzofulvene addend to the IBF–Ep scaffold, and IBF–Bis–Ep2 was prepared by the complete epoxidation of IBF–Bis. The structures of the synthesized compounds were characterized by ^{1}H, ^{13}C NMR, and mass spectrometry (detailed in supporting information). The syntheses and characterization of IBF–Mono and IBF–Ep can be found in a elsewhere.[14]

The thermal stabilities of our fullerenes and a PCBM standard were examined by thermogravimetric analysis (TGA) experiments over the range from 50 ^{o}C to 900 ^{o}C (Figure S2). In Figure S2 (a), PCBM displays the first thermal decomposition around 400 ^{o}C, whereas both IBF–Mono and IBF–Bis exhibit initial weight loss at lower temperatures of around 300 ^{o}C. We attribute this weight loss to retro-cycloaddition[18,19] and decomposition of the functional groups. The loss at higher temperatures

around 700–800 °C is likely the result of fullerene sublimation.[20] Figure S2 (b) reveals similar behavior of IBF–Ep, IBF–Bis–Ep1, and IBF–Bis–Ep2 with the first decomposition around 300–400 °C and sublimation at higher temperatures. It is notable that fullerene derivatives with isobenzofulvene moieties (IBF–Mono, IBF–Bis, IBF–Bis–Ep1) display two steps of functional group decomposition around 300–400 °C, while those with only epoxy moieties (IBF–Ep, IBF–Bis–Ep2) have a single step in the range. We can assume that the isobenzofulvene moiety undergoes a two-step process of thermal decomposition. The minor weight loss below 260 °C observed for IBF–Mono and IBF–Bis–Ep2 is likely a result of residual solvent, toluene, contained in the crystalline phase of the fullerenes, and similar behavior has been reported previously.[21]

Scheme 1. Synthesis of (a) IBF–Bis (b) IBF–Bis–Ep1 and (c) IBF–Bis–Ep2.

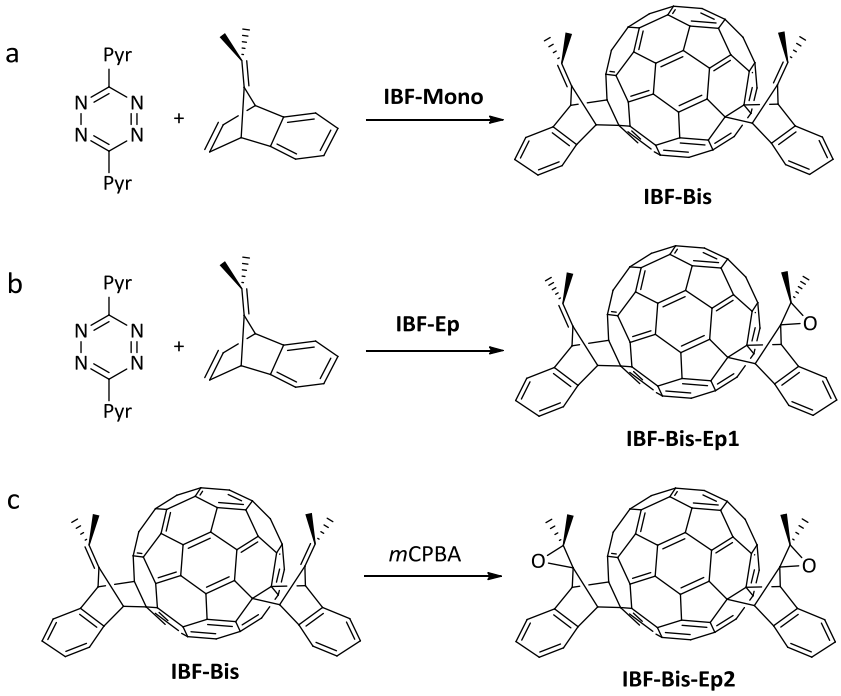

2.2. BHJ Photovoltaic Performance

We have investigated IBF–Mono, IBF–Bis, IBF–Ep, IBF–Bis–Ep1, and IBF–Bis–Ep2 (Figure 1 (a)) as electron acceptors in BHJ solar cells with P3HT as a donor, and have benchmarked their performance to P3HT:PCBM devices. The selection of P3HT as the benchmark polymer is a result of the high reproducibility of devices, and ongoing studies address the pairing of IBF–C_{60} acceptors with low-band gap polymers designed for higher efficiency. Experimental details of device fabrication can be found in the experimental section. A summary of the comparison between the performance of our reference P3HT:PCBM devices with those of reported in the literature is shown in Figure S3. The performance of our devices (current density as a function of applied voltage (*J*–*V*)) is shown in Figure 1 (b), and the relative parameters are listed in Table 1. Figure 1 (c) displays the distribution of V_{OC} in our devices with different acceptors and indicates that devices containing IBF–C_{60}s (except for IBF–Mono) exhibit a higher V_{OC} than conventional P3HT:PCBM devices. The broad distribution of V_{OC} in P3HT:IBF–Mono devices is a result of the poor solubility of IBF–Mono that lowers reproducibility. However, given the presence of high V_{OC} outliers for IBF–Mono suggests an intrinsic potential to produce high voltages. The J_{SC} in the devices with IBF–Mono or IBF–Bis is low, and is significantly improved by the epoxidation of isobenzofulvene moieties, as illustrated for both mono- and bisadducts in Figure 1 (b). The epoxidation of IBF–Mono, which creates IBF–Ep, improves both J_{SC} and V_{OC} resulting in a a PCE

of 3.1% which is a 20% increase from the standard efficiency (2.5%). P3HT:IBF–Ep devices also display high reproducibility as shown by the narrow V_{OC} distribution in Figure 1 (c).

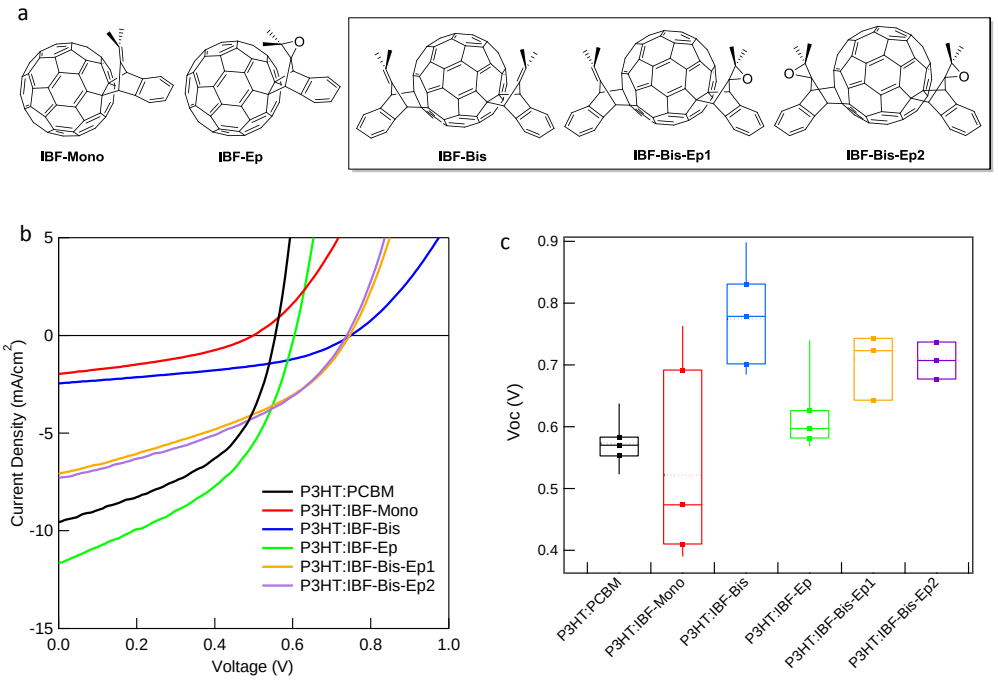

Figure 1. (a) Chemical structures of IBF–Mono5 IBF–Ep14 IBF–Bis, IBF–Bis–Ep1, and IBF– Bis–Ep2. New molecules reported in this paper are in the box. (b) Current density as a function of applied voltage for the fullerenes in BHJ architec-ture for solar cells with P3HT, compared to conventional P3HT:PCBM. (c) Box plot of the VOC values obtained from the devices in (b) where the whiskers indicate the 10th to 90th percentile and the box shows the 25th to 75th percentile con-taining the median (solid line) and average (dotted line). Ex-cept for P3HT:IBF–Mono, the median VOC for the devices with the new fullerenes are higher than conventional P3HT:PCBM devices.

Table 1. OPV characteristics of the devices in Figure 1 (b).

	IBF–Mono	IBF–Bis	IBF–Ep	IBF–Bis–Ep1	IBF–Bis–Ep2	PCBM
J_{SC} [mA/cm^2]	1.97	2.45	11.66	7.10	7.29	9.56
V_{OC} [V]	0.497	0.749	0.603	0.743	0.737	0.557
FF [%]	0.36	0.43	0.44	0.38	0.40	0.47
η [%]	0.36	0.78	3.10	2.02	2.12	2.52

Definitions: short-circuit current density, J_{SC}; open-circuit voltage, V_{OC}; fill factor, FF; PCE, η.

2.3. Understanding V_{OC} Differences

In order to determine the relative energy levels, we conducted cyclic voltammetry and UV–Vis absorption spectroscopy of IBF–C_{60} bisadducts.[22,23] Cyclic voltammetry reveals the relative reduction potentials of the C_{60} derivatives as shown in Figure 2 (a). As compared to PCBM, the reduction onset potential of IBF–Bis is lowered by 180 mV. This result is similar to ICBA, which possesses 170 mV lower reduction potential when compared to PCBM.[10] We hypothesize that the π–π interactions between the C_{60} surface and the attached functional groups (aromatic ring and double bond) contribute to the

large decreases in the electron affinity of fullerene. Epoxidation of IBF–Bis removes the π–π interaction between C_{60} and the pendant double bond. The reduced π–π interaction and the presence of the electron-withdrawing epoxide group manifest slightly increased electron affinity (less negative reduction potential) of IBF–Bis–Ep1 and IBF–Bis–Ep2 as marked by the dotted lines for visual aid in Figure 2 (a). The incorporation of epoxide groups thus lowers the LUMO energy levels relative to the IBF analogs. The comparative UV–Vis absorption spectra of our new fullerene derivatives and PCBM in solution are plotted over the range of 350–800 nm in Figure 2 (b). The bisadducts show longer onset wavelengths (smaller optical band gaps) and broader absorption characteristics than PCBM as a result of their regioisomeric mixtures. The bisadducts also have higher absorptivity as a result of their lowered symmetry. The optical band gaps are used to approximate the HOMO energy levels of the fullerenes by being subtracted from the LUMO levels derived from cyclic voltammetry. The values obtained from the aforementioned experiments are summarized in Table 2, and the MO energy level diagrams of the fullerenes along with the previously reported IBF–Mono and IBF–Ep[14] are depicted in Figure 2 (c).

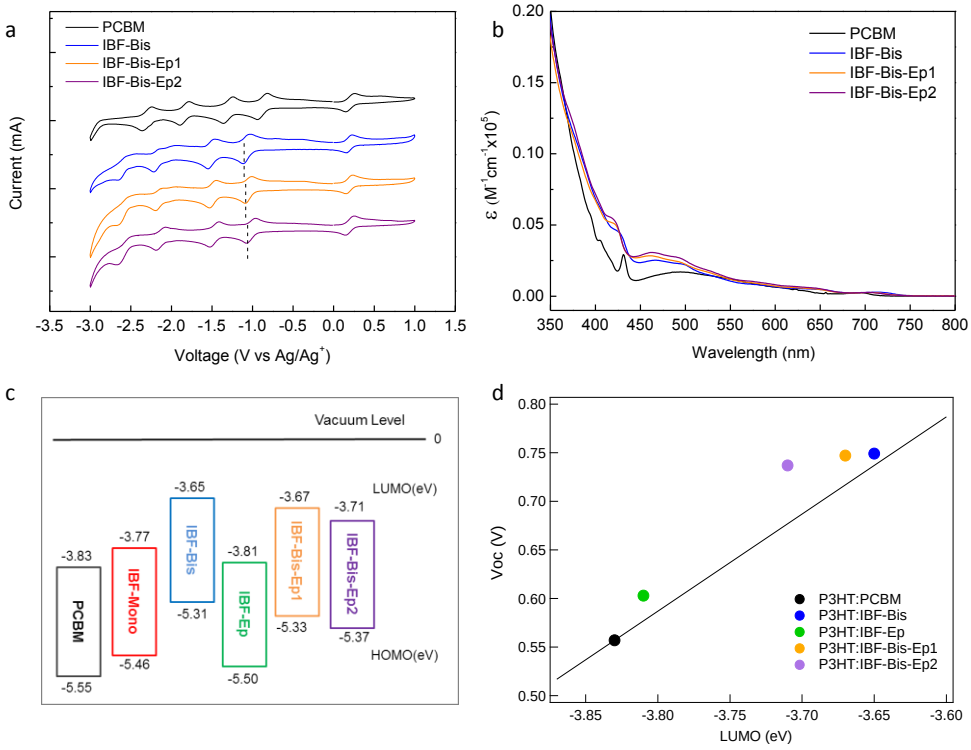

Figure 2. (a) Cyclic voltammograms of PCBM, IBF–Bis, IBF–Bis–Ep1, IBF–Bis–Ep2 (under N_2, 0.1 M Bu_4NPF_6 in toluene/acetonitrile (4:1), Pt (WE, 2.01 mm^2), Pt wire (CE), $Ag/AgNO_3$ (RE), scan rate 0.1 V/s, Fc/Fc^+ internal standard $E_{1/2}$ at 0.20 V). Cyclic voltammograms of IBF–Mono and IBF–Ep can be found in a previous report.[14] (b) UV–Vis absorption spectra of PCBM (2.4 x 10^{-5} M), IBF–Bis (2.4 x 10^{-5} M), IBF–Bis–Ep1 (2.4 x 10^{-5} M) and IBF–Bis–Ep2 (2.2 x 10^{-5} M) in $CHCl_3$. UV–Vis absorption spectra of IBF–Mono and IBF–Ep can be also found in the aforementioned paper.[14] (c) HOMO–LUMO energy diagrams of all functionalized fullerenes. Values for IBF–Mono and IBF–Ep are reported[14] for comparison. The MO energy levels were scaled relative to the vacuum level set to zero. (d) Measured V_{OC}s and the LUMO energy levels of fullerenes. The guideline passing through P3HT:PCBM data point predicts V_{OC} of other devices based on the LUMO levels of the respective fullerene acceptors relative to that of PCBM.

The larger V_{OC}s of the bisadducts are in accord with their raised LUMO levels, however all the V_{OC} values cannot be solely explained by their raised LUMO levels. All the IBF–C_{60}-based devices (except for IBF–Mono where the variation in the V_{OC} values prevents proper comparison) have higher V_{OC} as predicted (Figure 2 (d)) from their LUMO levels relative to PCBM. In order to best understand the origin

of the improved performance we undertook charge carrier recombination measurements. Transient photovoltage (TPV) and photocurrent (TPC) measurements evaluate charge carrier recombination under open circuit and relate V_{OC} to charge carrier recombination dynamics,[24,25] and our results are shown in Figure 3. P3HT:PCBM devices exhibit a shorter recombination lifetime compared to devices using our fullerenes at the same averaged photogenerated charge density. The slower recombination dynamics of IBF–C_{60}-based devices have the overall effect of increasing the V_{OC} compared to the values predicted solely by their LUMO energy levels. Previous reports have assigned non-geminate recombination processes to be the limiting mechanism for V_{OC} in P3HT:PCBM solar cells.[26–29] The similar recombination dynamics (e.g. similar power laws) in Figure 3 for both PCBM and IBF–C_{60}-based solar cells suggest that in all the tested devices non-geminate recombination is the limiting factor for V_{OC}. Since the non-geminate recombination is most likely to occur at the interface between the p- and n-type materials,[30] the slower recombination for IBF–C_{60}-based devices could suggest improved electronic interface behavior between IBF–C_{60} derivatives and P3HT compared to that with PCBM.[31] Also, the similar recombination lifetimes of all our IBF–C_{60}-based devices suggest their similar electronic/organizational features at the interface with P3HT. We conclude that the generation of large V_{OC} in P3HT:IBF–C_{60} devices is the result of a combination of increased LUMO levels and slower recombination dynamics.

Table 2. HOMO and LUMO energies of fullerene derivatives calculated from UV–Vis absorption and cyclic voltammetry

C_{60} derivative	E_1[V][a]	E_2[V]	E_3[V]	E_{onset}[V][b]	LUMO[eV][c]	λ_{onset}[nm][d]	HOMO[eV][e]	E_{gap}[eV][f]
PCBM	-0.87	-1.30	-1.83	-0.77	-3.83	723	-5.55	1.72
IBF–Mono[14]	-0.92	-1.33	-1.89	-0.83	-3.77	737	-5.46	1.69
IBF–Bis	-1.08	-1.51	-2.18	-0.95	-3.65	750	-5.31	1.66
IBF–Ep[14]	-0.88	-1.32	-1.87	-0.79	-3.81	733	-5.51	1.70
IBF–Bis–Ep1	-1.05	-1.49	-2.16	-0.93	-3.67	749	-5.33	1.66
IBF–Bis–Ep2	-1.02	-1.47	-2.14	-0.89	-3.71	749	-5.37	1.66

(a) Half-wave potential, 0.5 (Ep.a.+Ep.c.); Ep.a., anodic peak potential; Ep.c. cathodic peak potential; (b) Onset reduction potential; (c) LUMO (eV) = −e (E_{onset}+4.60); (d) Onset absorption wavelength; (e) HOMO = LUMO−E_{gap} [eV]; (f) Band gap = hc/λ_{onset} , converted [J] to [eV]; h, Planks constant; c, speed of light. Values for IBF–Mono and IBF–Ep are copied from the previous report[14] for comparison.

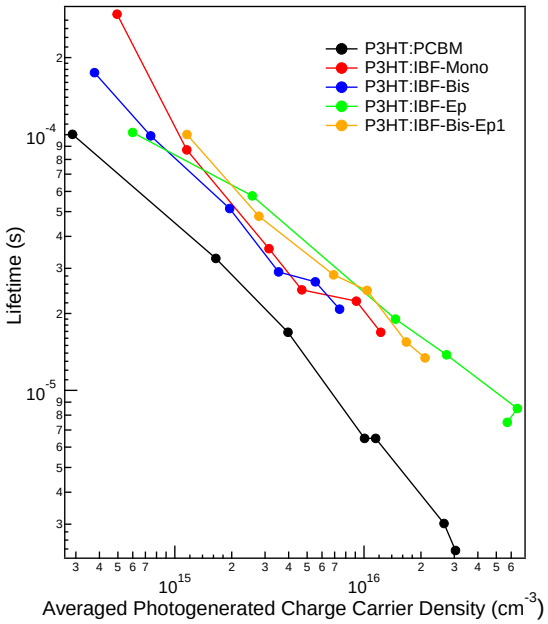

Figure 3. Recombination lifetime as a function of the averaged photogenerated charge carrier density measured with transient photovoltage and photocurrent (TPV/TPC).

2.4. Understanding J_{SC} Differences

To better understand the mechanisms determining the J_{SC} of our devices, we first measured their morphology by atomic force microscopy (AFM).[32] Topographic images at 1 μm scale in Figure 4 (a) show similar phase separation of donor and acceptor domains for all blends studied. They exhibit similar RMS roughness, with the exception of the P3HT:IBF–Mono blend where particles of IBF–Mono are present. The latter observation is consistent with the poor solubility of IBF–Mono and the low J_{SC} of the device. Figure 4 (b) at 10 μm scale further indicates the severe aggregation of IBF–Mono, as opposed to PCBM in the blends with P3HT. In order to understand the improved J_{SC} in devices with IBF–C_{60} epoxide derivatives, we examined the UV–Vis absorption and photoluminescence (PL) of thin films fabricated under the same conditions as used for the devices in Figure 1 (b).[33] The UV–Vis absorption spectra of thin films plotted in Figure 5 (a) reveal the reduced absorption in devices with IBF–C_{60}s compared to P3HT:PCBM at equal thickness. The P3HT:IBF–Mono device particularly exhibits higher PL in Figure 5 (b), which indicate more radiative recombination as compared to other blends with more quenched emission. These PL characteristic of P3HT:IBF–Mono film is consistent with its low $J_{SC.}$and less effective BHJ structure.[34] Finally, we believe that the high J_{SC} of P3HT:IBF–Ep device is attributed to its higher charge carrier density compared to that in P3HT:PCBM reference devices. This is supported by the higher averaged photogenerated charge carrier density of P3HT:IBF–Ep devices ($4.8x10^{16}$ cm^{-3}) as compared to P3HT:PCBM devices ($2.0x10^{16}$ cm^{-3}) under open-circuit at the light intensity of 1 Sun (Figure S4). With the aid of a simple analytical diode model, it is possible to calculate the predicted J_{SC} obtained by increasing the charge carrier density at open-circuit).[1] We predicted the J_{SC} of P3HT:IBF–Ep devices to be 11.2 $mAcm^{-2}$, which is in agreement with the experimental value in Table 2 (11.66 $mAcm^{-2}$). Similarly, the averaged photogenerated charge carrier density at open circuit of P3HT:IBF–Bis–Ep1 ($1.4x10^{16}$ cm^{-3}) is higher than that of P3HT: IBF–Bis ($4.7x10^{15}$ cm^{-3}), which is in line with the higher J_{SC} of P3HT:IBF–Bis–Ep1 as compared to P3HT:IBF–Bis. These results confirm that J_{SC} of devices can be influenced collectively by morphology, light absorption, radiative recombination, and photogenerated charge carrier density in devices.

[1] This model based on the formula $Voc = \frac{nkT}{q} ln(\frac{Jsc}{J0})$ where *n* is the non-ideality factor, *k* the Boltzmann constant, *T* the temperature and J_0 the saturation current assumes similar diode characteristics (J_0 and *n* = 1.4) for P3HT:IBF–Ep and P3HT:PCBM devices with the aim of providing an approximate prediction of $J_{SC.}$

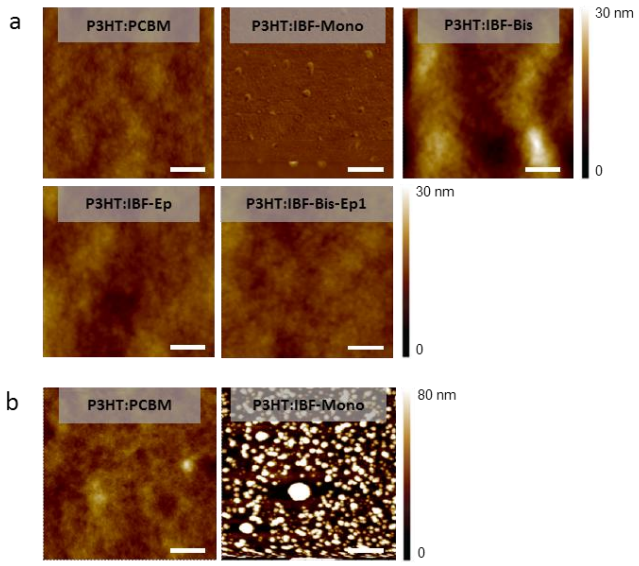

Figure 4. AFM topographic images of the devices analyzed in this study at (a) 1 μm and (b) 10 μm scales. The scale bars measure 200 nm in (a) and 2 μm in (b). The topography at 1 μm scale in (a) shows similar phase separation for all the blends under study, except for P3HT:IBF–Mono where particles are observed. The root-mean-square (RMS) roughness measured on each film is 3.5 nm (PCBM), 20.0 nm (IBF–Mono), 2.5 nm (IBF–Bis), 3.0 nm (IBF–Ep), and 10.4 nm (IBF–Bis–Ep1). 10 μm scale images in (b) also show significant amount of the particles of IBF–Mono that are not fully dissolved.

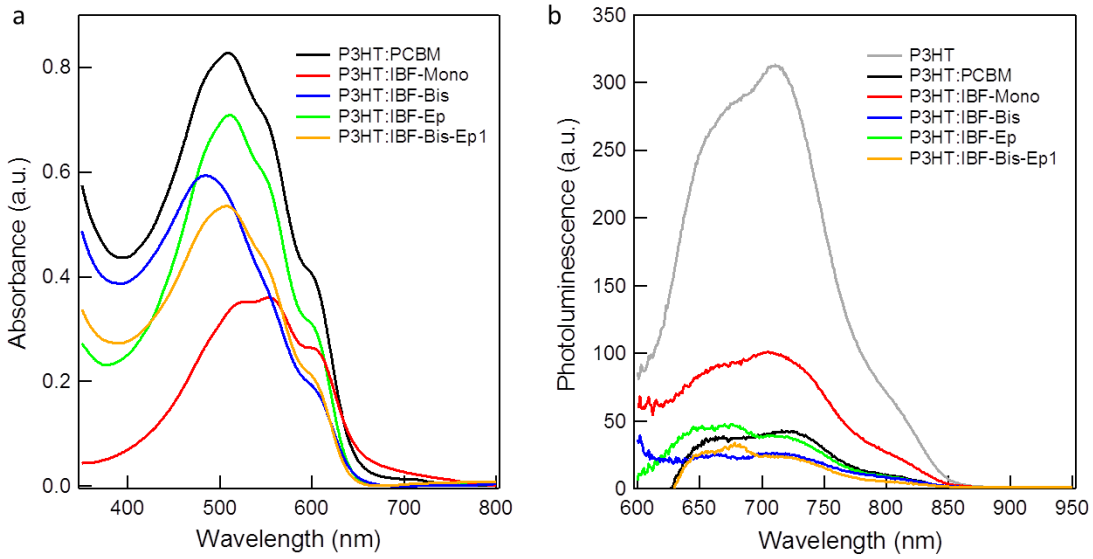

Figure 5. Optical characterization of the devices studied. Due to the similar results of IBF–Bis–Ep1 and IBF–Bis–Ep2, only IBF–Bis–Ep1 is shown for simplicity. (a) Steady-state spectral UV–Vis absorption of thin films fabricated under the same conditions as used for the devices in Figure 1 (b) and normalized for thickness. (b) Steady-state spectral photoluminescence (PL) emission of thin films fabricated under the same conditions as used for the devices in Figure 1 (b). Films were excited with monochromatic light at 500 nm and normalized for absorption. All fullerenes quench PL when blended with P3HT, though P3HT:IBF–Mono shows higher level of radiative exciton recombination that could result in low J_{SC}.

3. Conclusion

A series of isobenzofulvene–C_{60} derivatives were designed and examined as electron acceptors in BHJ solar cells with a P3HT donor and produced higher V_{OC} than PCBM as a result of significant cofacial π–interactions in the molecules that raised LUMO energy levels. The isobenzofulvene–C_{60} derivatives also exhibited desirably slower recombination dynamics in the devices relative to PCBM, which also contributes to generating high V_{OC}. The epoxide derivatives showed improved solubility as well as increased J_{SC} in photovoltaic devices. The concomitant increase of V_{OC} and J_{SC} observed for P3HT:IBF–Ep devices relative to P3HT:PCBM standard cells resulted in ~20% enhancement of PCE. Ongoing studies are directed at pairing these acceptors with low-band gap polymers to produce high efficiency solar cells.

4. Experimental Methods

4.1. Materials. C_{60} was purchased from SES Research. $PC_{61}BM$, and P3HT were purchased from Sigma–Aldrich. PEDOT:PSS were purchased from Ossila. 3,6-Di-2-pyridyl-1,2,4,5-tetrazine was purchased from Alfa Aesar. All the compounds purchased from commercial sources were used as received. Other materials including solvents and electrolyte salt were commercially available.

4.2. Measurements. Reaction mixtures containing multiadducts of fullerenes were separated by 5PBB Cosmosil column (10 mm x 250 mm) from Nacalai Tesque, Inc. installed in Agilent Technologies ProsStar 210 High Pressure Liquid Chromatography (HPLC) system. ^{1}H and ^{13}C NMR spectra were taken on Varian Inova–500 spectrometers. Chemical shifts were reported in ppm and referenced to residual solvent peaks (CD_2Cl_2: 5.33 ppm for ^{1}H, 53.84 ppm for ^{13}C, CS_2: 192.92 ppm for ^{13}C). Bruker Daltonics Omniflex MALDI–TOF mass spectrometer was used for mass determination without the use of a matrix. UV–Vis absorption spectra were obtained using a Cary 4000 UV-Vis spectrophotometer. Electrochemical measurements were carried out in a glove box under nitrogen, using an Autolab PGSTAT 10 or PGSTAT 20 potentiostat (Eco Chemie) in a three-electrode cell configuration. A Pt button (1.6 mm in diameter) electrode, a Pt wire, and a quasi-internal Ag wire submerged in 0.01M $AgNO_3$/0.1M tetrabutylammonium hexafluorophosphate ($TBAPF_6$) in acetonitrile were used as a working electrode, a counter electrode, and a reference electrode, respectively, in 0.1M $TBAPF_6$ toluene/acetonitrile (4:1) solution. The ferrocene/ferrocenium (Fc/Fc^{+}) redox couple was used as an internal standard, with the half-wave potentials observed between 0.193–0.205 V vs Ag/Ag^{+} in toluene/acetonitrile (4:1) solution. Thermogravimetric Analyses were performed with a Discovery TGA (TA Instruments) under nitrogen. Samples were heated at 20^{o} C/min from 50^{o} C to 900^{o} C.

4.3. Device Fabrication. Pre-patterned indium tin oxide (ITO)-coated glass substrates (Thin Film Devices, Inc.) were sonicated in deionized water (10 min), acetone (10 min) and isopropanol (10 min) and oxygen plasma-cleaned (3 min) immediately prior to deposition of the PEDOT:PSS layer. PEDOT:PSS (2–5 wt% in water) was spin-coated at 4000 rpm and annealed at 150 °C (using a hotplate) for 20 min. For the active layer, a 25 mg/mL solution of P3HT:fullerene with an optimized ratio varying from 1: 0.5 to 1:1 in chlorobenzene (CB) was spin-coated onto the PEDOT:PSS layer at 1000 rpm under nitrogen and annealed on a 150 °C hotplate for 20 min under nitrogen. Finally, 25 nm Ca followed by 100 nm Al electrode was deposited by thermal evaporation.

4.4. Device Characterization. Current density–voltage (*J*–*V*) measurements were recorded by a Keithley 6487 picoammeter both in the dark and under illumination. The devices were illuminated through the glass substrate using an Oriel 91191 150 W full spectrum solar simulator. The illumination intensity was calibrated to 100 mW/cm^2 using an NREL-certified silicon photodiode. The optical absorption and photoluminescence spectra of devices were obtained by using a Cary 5E UV-vis-NIR dual-beam spectrophotometer. Transient photocurrents and recombination lifetime measurement were conducted with a Newport laser diode (830 nm) driven by an Agilent 33220. A function generator was used as a second light source to provide square wave modulated illumination. This illumination was filtered through a neutral density filter before reaching the device to ensure a small illumination perturbation. V_{OC} decay transients were recorded on a Tektronix TDS 3054B digital oscilloscope.

ASSOCIATED CONTENT

Supporting Information

Synthetic procedures, 1H and 13C NMR spectra, TGA data of the reported molecules, standard device (P3HT:PCBM) performance distribution compared to the reported values in the literature, and averaged photogenerated charge carrier density as a function of the light intensity for all the blends studied. The Supporting Information is available free of charge on the ACS Publications website.

ACKNOWLEDGMENT

This work was supported by Eni SpA under the Eni-MIT Solar Frontiers Center

REFERENCES

[1] G. Yu, J. Gao, J.C. Hummelen, F. Wudl, A.J. Heeger, Polymer Photovoltaic Cells - Enhanced Efficiencies Via a Network of Internal Donor-Acceptor Heterojunctions, Science (80-.). 270 (1995) 1789–1791.

[2] J. Chen, Y. Cao, Development of Novel Conjugated Donor Polymers for High-Efficiency Bulk-Heterojunction Photovoltaic Devices, Acc. Chem. Res. 42 (2009) 1709–1718.

[3] R. Jean, Molecular bulk heterojunctions: An emerging approach to organic solar cells, Acc. Chem. Res. 42 (2009) 1719–1730. doi:10.1021/ar900041b.

[4] B.C. Thompson, J.M.J. Frechet, Organic photovoltaics - Polymer-fullerene composite solar cells, Angew. Chemie-International Ed. 47 (2008) 58–77.

[5] M.C. Scharber, D. Wuhlbacher, M. Koppe, P. Denk, C. Waldauf, A.J. Heeger, et al., Design rules for donors in bulk-heterojunction solar cells - Towards 10 % energy-conversion efficiency, Adv. Mater. 18 (2006) 789–794.

[6] C.J. Brabec, A. Cravino, D. Meissner, N.S. Sariciftci, T. Fromherz, M.T. Rispens, et al., Origin of the open circuit voltage of plastic solar cells, Adv. Funct. Mater. 11 (2001) 374–380.

[7] Y.-J. Cheng, S.-H. Yang, C.-S. Hsu, Synthesis of Conjugated Polymers for Organic Solar Cell Applications., Chem. Rev. (2009) 5868–5923. doi:10.1021/cr900182s.

[8] D. Muhlbacher, M. Scharber, M. Morana, Z.G. Zhu, D. Waller, R. Gaudiana, et al., High photovoltaic performance of a low-bandgap polymer, Adv. Mater. 18 (2006) 2884–2889.

[9] C.L. Chochos, N. Tagmatarchis, V.G. Gregoriou, Rational design on n-type organic materials for high performance organic photovoltaics, RSC Adv. (2013) 1–22. doi:10.1039/c3ra22926b.

[10] Y. He, H.Y. Chen, J. Hou, Y. Li, Indene - C60 bisadduct: A new acceptor for high-performance polymer solar cells, J. Am. Chem. Soc. 132 (2010) 1377–1382. doi:10.1021/ja908602j.

[11] Y. Zhang, Y. Matsuo, C.Z. Li, H. Tanaka, E. Nakamura, A scalable synthesis of methano[60]fullerene and congeners by the oxidative cyclopropanation reaction of silylmethylfullerene, J. Am. Chem. Soc. 133 (2011) 8086–8089. doi:10.1021/ja201267t.

[12] G.D. Han, W.R. Collins, T.L. Andrew, V. Bulović, T.M. Swager, Cyclobutadiene–C60 Adducts: N-Type Materials for Organic Photovoltaic Cells with High Voc, Adv. Funct. Mater. 23 (2013) 3061–3069. doi:10.1002/adfm.201203251.

[13] N.-W. Tseng, Y. Yu, Y. Li, J. Zhao, S.K. So, H. Yan, et al., Isobenzofulvene-fullerene mono-adducts for organic photovoltaic applications, J. Mater. Chem. C Mater. Opt. Electron. Devices. 3 (2015) 977–980. doi:10.1039/C4TC02373K.

[14] S. Chang, H.G. Ddeul, J.G. Weis, H. Park, T.M. Swager, S. Gradečak, Ambient-Processed Transition Metal Oxide Free-Perovskite Solar Cells Enabled by a New Organic Charge Transport Layer, Submitted. (2015).

[15] H. Tanida, T. Irie, K. Tori, Generation and Cycloaddition of 8,8-Dimethylisobenzofulvene, Bull. Chem. Soc. Jpn. 45 (1972) 1999–2003. doi:10.1246/bcsj.45.1999.

[16] Y. Li, Fullerene-bisadduct acceptors for polymer solar cells, Chem. - An Asian J. 8 (2013) 2316–2328. doi:10.1002/asia.201300600.

[17] M. Lenes, G. Wetzelaer, F.B. Kooistra, S.C. Veenstra, J.C. Hummelen, P.W.M. Blom, Fullerene bisadducts for enhanced open-circuit voltages and efficiencies in polymer solar cells, Adv. Mater. 20 (2008) 2116–2119.

[18] J.L. Delgado, F. Oswald, F. Cardinali, F. Langa, N. Martìn, On the Thermal Stability of [60] Fullerene Cycloadducts : Retro-Cycloaddition Reaction of 2-Pyrazolino [4,5:1,2][60] fullerenes, J. Org. Chem. 73 (2008) 3184–3188. doi:10.1039/b717218d.

[19] N. Martín, M. Altable, S. Filippone, A. Martín-Domenech, L. Echegoyen, C.M. Cardona, Retro-Cycloaddition Reaction of Pyrrolidinofullerenes, Angew. Chemie Int. Ed. 45 (2006) 110–114. doi:10.1002/anie.200502556.

[20] H.H.N. J. Milliken, T. M. Keller, A. P. Baronavski, S. W. Mcelvany, J. H. Callahan, Thermal and Oxidative Analyses of Buckminsterfullerene, C60., Chem. Mater. (1991) 386–387.

[21] B.W. Larson, J.B. Whitaker, A. a. Popov, N. Kopidakis, G. Rumbles, O. V. Boltalina, et al., Thermal [6,6] → [6,6] isomerization and decomposition of PCBM (phenyl-C61-butyric acid methyl ester), Chem. Mater. 26 (2014) 2361–2367. doi:10.1021/cm500594u.

[22] P.P. Khlyabich, B. Burkhart, B.C. Thompson, Efficient Ternary Blend Bulk Heterojunction Solar Cells with Tunable Open-Circuit Voltage, J. Am. Chem. Soc. 133 (2011) 14534–14537. doi:10.1021/ja205977z.

[23] F.B. Kooistra, J. Knol, F. Kastenberg, L.M. Popescu, W.J.H. Verhees, J.M. Kroon, et al., Increasing the open circuit voltage of bulk-heterojunction solar cells by raising the LUMO level of the acceptor, Org. Lett. 9 (2007) 551–554. doi:10.1021/ol062666p.

[24] A. Maurano, R. Hamilton, C.G. Shuttle, A.M. Ballantyne, J. Nelson, B. O'Regan, et al., Recombination Dynamics as a Key Determinant of Open Circuit Voltage in Organic Bulk Heterojunction Solar Cells: A Comparison of Four Different Donor Polymers, Adv. Mater. 22 (n.d.) 4987–4992.

[25] A. Maurano, C.C. Shuttle, R. Hamilton, A.M. Ballantyne, J. Nelson, W.M. Zhang, et al., Transient Optoelectronic Analysis of Charge Carrier Losses in a Selenophene/Fullerene Blend Solar Cell, J. Phys. Chem. C. 115 (n.d.) 5947–5957.

[26] C.G. Shuttle, B. O'Regan, A.M. Ballantyne, J. Nelson, D.D.C. Bradley, J.R. Durrant, Bimolecular recombination losses in polythiophene: Fullerene solar cells, Phys. Rev. B. 78 (2008) 4.

[27] A. Pivrikas, G. Juska, A.J. Mozer, M. Scharber, K. Arlauskas, N.S. Sariciftci, et al., Bimolecular recombination coefficient as a sensitive testing parameter for low-mobility solar-cell materials, Phys. Rev. Lett. 94 (2005) 4.

[28] L.J.A. Koster, E.C.P. Smits, V.D. Mihailetchi, P.W.M. Blom, Device model for the operation of polymer/fullerene bulk heterojunction solar cells, Phys. Rev. B. 72 (2005) 9.

[29] D. Rauh, C. Deibel, V. Dyakonov, Charge Density Dependent Nongeminate Recombination in Organic Bulk Heterojunction Solar Cells, Adv. Funct. Mater. 22 (2012) 3371–3377. doi:10.1002/adfm.201103118.

[30] C. Deibel, V. Dyakonov, Polymer-fullerene bulk heterojunction solar cells, Reports Prog. Phys. 73 (n.d.) 39.

[31] D. Credgington, J.R. Durrant, Insights from Transient Optoelectronic Analyses on the Open-Circuit Voltage of Organic Solar Cells, J. Phys. Chem. Lett. 3 (2012) 1465–1478. doi:10.1021/jz300293q.

[32] S.E. Shaheen, C.J. Brabec, N.S. Sariciftci, F. Padinger, T. Fromherz, J.C. Hummelen, 2.5% efficient organic plastic solar cells, Appl. Phys. Lett. 78 (2001) 841–843.

[33] P. a Troshin, H. Hoppe, A.S. Peregudov, M. Egginger, S. Shokhovets, G. Gobsch, et al., [70]Fullerene-Based Materials for Organic Solar Cells., ChemSusChem. 4 (2011) 119–124. doi:10.1002/cssc.201000246.

[34] T.M. Clarke, J.R. Durrant, Charge Photogeneration in Organic Solar Cells, Chem. Rev. 110 (2010) 6736–6767.

Graphical abstract

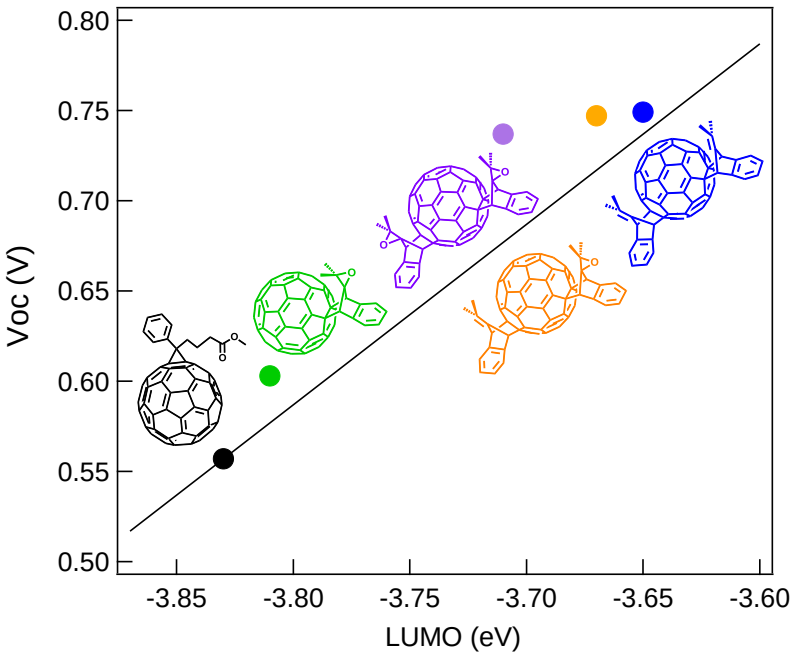

Supplementary MATLAB .fig files

Click here to download Supplementary MATLAB .fig files: IBF_SI.pdf